EUROPHYSICS LETTERS 1 September 2000

Europhys. Lett., **51** (5), pp. 485–491 (2000)

Observation of interaction dynamics in finite-temperature Bose condensed atom clouds

B. D. Busch[1,2], Chien Liu[1], Z. Dutton[1,2], C. H. Behroozi[1,3] and L. Vestergaard Hau[1,2]

[1] *Rowland Institute for Science - Cambridge MA, 02142, USA*
[2] *Department of Physics, Harvard University - Cambridge MA 02138, USA*
[3] *Division of Engineering and Applied Sciences, Harvard University Cambridge MA 02138, USA*

(received 24 May 2000; accepted 29 June 2000)

PACS. 03.75.Fi – Phase coherent atomic ensembles; quantum condensation phenomena.
PACS. 05.30.Jp – Boson systems.

Abstract. – We present measurements of finite-temperature atom clouds cooled below the transition temperature for Bose-Einstein condensation. We study the dynamics of the interface region between the Bose condensed and noncondensed components of the atom clouds, where the time-dependent density profile is highly sensitive to interactions between the two components. We observe directly the effects of repulsion from the condensate on the dynamics of noncondensed atoms. The measurements are compared to calculations based on Hartree-Fock-Bogoliubov mean-field theory. We infer a value for the spatial second-order correlation function for noncondensed atoms of $g^{(2)}_{0,\mathrm{NC}}(\boldsymbol{r}=0) = 1.8 \pm 0.3$.

The experimental observation of Bose-Einstein condensates (BEC) in 1995 [1–3] has been followed by intense studies of condensate properties [4]. In this paper we focus on the dynamics of the noncondensed component of a finite-temperature atom cloud cooled below the transition temperature for Bose-Einstein condensation. We present data and calculations that clearly reveal the repulsive interaction between the condensate and the noncondensed atoms in clouds released from a magnetic trap. The interface region between the two components is particularly sensitive to such interaction effects and we have used near-resonant absorption imaging to precisely probe this region. To describe the dynamics we have developed a theoretical model within the mean-field Hartree-Fock-Bogoliubov approximation [5, 6], that accounts for the interaction between the two components. We speculate that our model could be used also for studies of collective excitations in finite-temperature clouds, where an interesting discrepancy between theory and experiment remains [7–12]. From our observations we deduce a value of $g^{(2)}_{0,\mathrm{NC}}(\boldsymbol{r}=0) = 1.8 \pm 0.3$ for the second-order spatial correlation function for noncondensed atoms. This value is larger by a factor of ~ 2 than the corresponding value obtained for a condensate [13, 14].

The apparatus used to create the atom clouds is similar to the one described in refs. [15, 16]. We cool clouds with several million sodium atoms to temperatures below the critical

temperature for BEC and obtain densities above 10^{14} atoms/cm^3. To confine the atoms we use the 4-Dee trap, which results in a cylindrically symmetric harmonic potential, with an adjustable aspect ratio. The data presented here are for a trap with oscillator frequencies of $f_z = 28.0 \pm 0.1$ Hz along the axis of symmetry and $f_x = f_y = 504 \pm 10$ Hz in the two tightly confining directions. This leads to an atom cloud with an aspect ratio of 18:1. The clouds are abruptly released from the trap by turning off the confining magnetic fields in 400 μs, well below the trap's lowest oscillation period of 2 ms.

At a precisely adjustable time after release, a probe pulse with a duration of 10 μs is sent through the atom cloud. The probe laser is tuned near the $3S$, $F = 2 \rightarrow 3P$, $F = 3$ hyperfine transition within the D_2 manifold. Prior to that, the atoms are pumped from their original state, $|3S,\ F = 1\rangle$, to $|3S,\ F = 2\rangle$ for 10 μs by laser beams tuned to the $3S$, $F = 1 \rightarrow 3P$, $F = 2$ transition (the pump beams are left on during the probe pulse). The transmission profile of the probe laser is imaged onto a charge-coupled-device (CCD) camera and a second probe image is taken 65 ms after each main image to normalize out spatial intensity nonuniformities in the probe. The time delay of 65 ms is chosen to allow time for the atom cloud to diffuse to imperceptible densities, and is still short enough to ensure that the probe beam remains stable between images.

The imaging optics used to observe the expanding cloud consist of a pair of main lenses with a high numerical aperture and a pair of secondary magnifying lenses. The main lenses are 50 mm in diameter and the first is placed 250 mm away from the atom cloud, providing diffraction-limited performance at $f/5$. A CCD camera with a pixel size of 22.5 μm square is placed in the image plane of the lens system. Each pixel corresponds to 3.476 ± 0.005 μm in the object plane, as calibrated using a Ronchi ruling. The system's resolution has been verified to be 5 μm using a resolution target. The atom cloud is illuminated from below by the probe laser beam. To keep the images of the released (and falling) clouds focused, the first lens is mounted on a translation stage which is adjusted according to the flight time.

The rapid turn-off (400 μs) of the trapping magnets induces eddy currents in the vacuum chamber walls and copper gaskets. To avoid zero-crossings of the magnetic field at all times, and thereby avoid Majorana spin-flips in the atom cloud, we add a positive bias field 300 μs before the turn-off. This allows for accurate modeling of cloud dynamics during the magnetic field turn-off. By thus increasing the bias field to 100 Gauss over 400 μs, we also effectively turn off the transverse (x, y) confinement more abruptly than would a simple 400 μs ramp-down of the 4-Dee magnets, since the spring constant in the transverse directions is inversely proportional to the bias field.

To model the expansion of the atom cloud, we use the Hartree-Fock-Bogoliubov (HFB) mean-field approach [5,6,17]. The dynamics of the condensate are described by the generalized Gross-Pitaevskii equation

$$\frac{i\hbar\partial\Phi(\boldsymbol{r},t)}{\partial t} = \left(\frac{-\hbar^2\nabla^2}{2m} + V(\boldsymbol{r},t) + U_0 n_{\mathrm{C}}(\boldsymbol{r},t) + 2U_0 n_{\mathrm{T}}(\boldsymbol{r},t)\right)\Phi(\boldsymbol{r},t)\,, \tag{1}$$

where $\Phi(\boldsymbol{r},t)$ is the condensate "wave function" (the nonvanishing expectation value of the atomic field operator), $n_{\mathrm{C}} = |\Phi|^2$ is the condensate density, and n_{T} is the density of noncondensed atoms. The coupling constant U_0 is given by $U_0 = 4\pi\hbar^2 a/m$, where a is the scattering length and m the atomic mass (for the scattering length we use $a = 27.5$ Å [18]). $V(\boldsymbol{r},t)$ is the external potential from the magnetic field where we include a detailed model of eddy-current induced fields caused by trap turn-off.

We model the dynamics of the noncondensed component after trap release by using a classical Monte Carlo calculation. In the Hartree-Fock approximation, each noncondensed

atom experiences a time-dependent force due to the magnetic potential $V(\boldsymbol{r},t)$ *and* the mean-field potential from the condensate. This results in the following equation of motion:

$$\mathrm{d}\boldsymbol{p}/\mathrm{d}t = -\nabla\left(V(\boldsymbol{r},t) + 2\,U_0\,n_{\mathrm{C}}(\boldsymbol{r},t)\right)\,, \tag{2}$$

where $\boldsymbol{p}$ is the momentum of a noncondensed atom. This model does not include interactions between noncondensed atoms, which are negligible at the densities used in this experiment [19].

The initial thermodynamic state of the trapped cloud is determined by the measured number of atoms in the condensate and noncondensed components. The initial condensate wave function, $\Phi(\boldsymbol{r},t=0)$, and the six-dimensional phase space density for the noncondensed atoms, $f_{\mathrm{T}}(\boldsymbol{r},\boldsymbol{p},t=0)$ are generated by the HFB mean-field approach of Giorgini *et al.* [6]. The condensate wave function is obtained by the stationary version of eq. (1) [20],

$$\left(\frac{-\hbar^2\nabla^2}{2m} + V(\boldsymbol{r},0) + U_0 n_{\mathrm{C}}(\boldsymbol{r},0) + 2U_0 n_{\mathrm{T}}(\boldsymbol{r},0)\right)\Phi(\boldsymbol{r},0) = \mu\Phi(\boldsymbol{r},0)\,, \tag{3}$$

where μ is the chemical potential. The phase space density for the noncondensed atoms is obtained by using a semiclassical WKB approximation for the excited Bogoliubov modes. The procedure is iterative and as the initial guess for the condensate wave function, we use the parabolic shape obtained within the Thomas-Fermi approximation [21] in the absence of noncondensed atoms ($T=0$). We calculate $f_{\mathrm{T}}(\boldsymbol{r},\boldsymbol{p},0)$ with this approximation for the condensate wave function, and obtain the spatial density $n_{\mathrm{T}}(\boldsymbol{r},0)$ for use in eq. (3) by integrating $f_{\mathrm{T}}(\boldsymbol{r},\boldsymbol{p},0)$ over momentum coordinates. The refined solution for the condensate wave function is generated by the split-operator method [22] by evolving eq. (1) in imaginary time and relaxing the initial parabolic density distribution into the actual distribution $n_{\mathrm{C}}(\boldsymbol{r},0)$. The number of atoms determines the normalization of the wave function and thereby the chemical potential. The process typically converges after three iterations. Constraining the number of noncondensed atoms in the model to match the observed number determines the temperature.

With these initial conditions the dynamics of the atom cloud after trap turn-off are evaluated iteratively. For the Monte Carlo calculation, used to model the time evolution of the noncondensed atom density $n_{\mathrm{T}}(\boldsymbol{r},t)$, we use several million atoms distributed according to the initial, semiclassical phase space density. For the first evaluation of $n_{\mathrm{T}}(\boldsymbol{r},t)$ we use eq. (2) neglecting the presence of the condensate. The result is applied in eq. (1) and the time dependence of the condensate wave function is calculated with the split operator technique. Subsequently the condensate density $n_{\mathrm{C}}(\boldsymbol{r},t)$ is inserted in eq. (2) and an improved noncondensed atom density as a function of time is obtained. The iteration process has typically converged at this point [23].

We evaluate the transmission profile of the probe laser beam through a model cloud with an atom density given as a superposition of the calculated condensate and noncondensate densities. The transmission profile is numerically propagated through the $f/5$ imaging optics, which has little effect on the result.

Figure 1 shows a measured, normalized transmission profile of a two-component cloud imaged 6 ms after trap turn-off with a resonant probe laser pulse. Fitting the tails of the image to a Bose-Einstein distribution, we measure $N_{\mathrm{T}} = (1.59 \pm 0.05) \times 10^6$ noncondensed atoms (within the quoted error bars, the number of atoms obtained is independent of the exact model for the noncondensed atom density). The number of atoms in the condensate is determined to be $N_{\mathrm{C}} = (0.95 \pm 0.03) \times 10^6$ by first subtracting the fitted Bose-Einstein distribution from the two-component image, and then fitting the residue to a Thomas-Fermi parabolic shape with a smoothed surface [23], where the condensate number is the only free

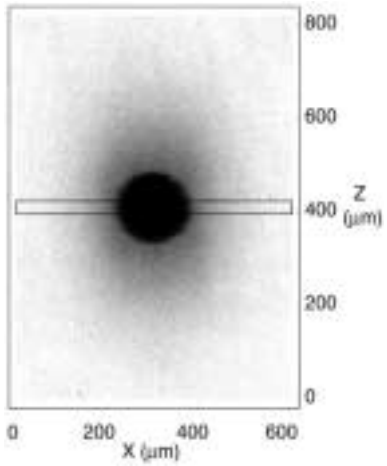

Fig. 1 – Normalized CCD image of a two-component cloud, taken after 6 ms of expansion. Black = 0%, white = 100% transmission.

parameter. The deduced numbers of atoms for the two components imply a temperature of $T = 890\,\mathrm{nK}$, a chemical potential $\mu = 0.35\,k_\mathrm{B}T$, and a critical temperature $T_\mathrm{c} = 1200\,\mathrm{nK}$ [24].

From the normalized transmission we may obtain the column density profile of the atom cloud. The transmission is $T = e^{-OD}$, where the optical density OD is the product of the column density and the absorption cross-section of the probe laser. The OD and column density corresponding to fig. 1 are shown in fig. 2 along the x-direction. Also shown in the figure is a solid curve resulting from a calculation where we used the model outlined above. There is excellent agreement with the data points. We have included a dashed curve which is obtained by neglecting interactions between the condensate and the noncondensed atoms. This model severely underestimates the density of the noncondensed component at the interface region, as is particularly clearly seen in fig. 2(b). The χ^2 value, obtained for the interface region marked in figs. 2(a)-(b), is 1.2 for the model including interactions and 31 for the interaction-free model. This is a direct observation of the repulsive interaction between the condensed and noncondensed components.

The error bars included in the figures and used in the χ^2 evaluation represent the uncertainty on the *difference* between the model and the data (for fig. 2, the error bars are approximately the size of the dots indicating the data points). They are calculated starting from the uncertainty of $\delta N_\gamma = \sqrt{N_\gamma}$ in the number of photons N_γ per CCD pixel. These photons are incident on a portion of the cloud with column density $N_\mathrm{at}/(\mathrm{d}x\,\mathrm{d}z)$, where N_at is the number of atoms within a column of area $(\mathrm{d}x\,\mathrm{d}z)$ corresponding to the area of a CCD pixel at the position of the cloud. The column density has an associated uncertainty $\sqrt{N_\mathrm{at}}/(\mathrm{d}x\,\mathrm{d}z)$ [25], which adds to the uncertainty in the number of photons after the cloud. These photons are converted to photo-electrons with a quantum efficiency $p \approx 0.4$, and then digitized with an analog-to-digital converter (ADC) gain of $G_\mathrm{ADC} = 0.42\,\mathrm{ADC}$ counts per photo-electron, and a readout noise of 3 ADC counts per pixel. We further include a term proportional to the number of photons incident on a pixel, to account for the observed noise due to interference fringes in the probe beam, which are not completely cancelled out by the normalization image. Finally, since we are comparing our data to a Monte Carlo image with a finite number of model atoms (5×10^6), there is a small term to account for statistical fluctuations in the Monte Carlo distribution.

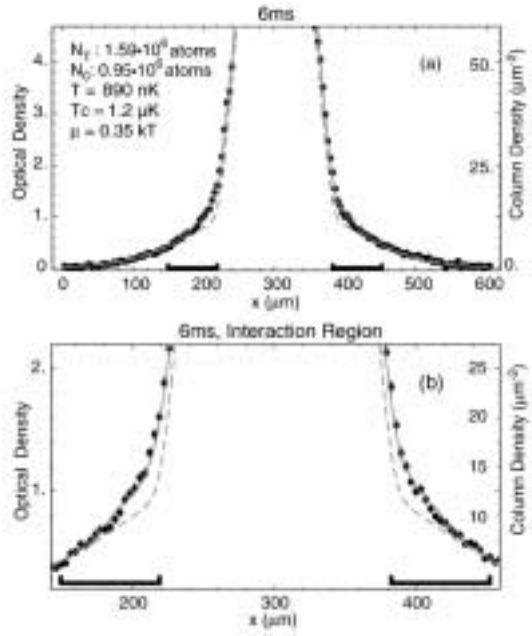

Fig. 2 – (a) Cross-section along the x-axis through the cloud of fig. 1. The data (black points) are compared to a calculation (solid curve) where interactions between the condensate and noncondensed component are included through a mean-field potential. For the model used here, we include the full quantum-mechanical exchange interaction corresponding to eqs. (1) and (2). We also compare to a model (dashed curve) where we neglect interactions between the condensed and noncondensed components. Each data point along the cross-sections is the result of an average over 9 pixels in the z-direction, as indicated by the boxed-in area of fig. 1. N_{T} and N_{C} indicated in the figure are the number of atoms in the noncondensed and condensed components, respectively. (b) An expanded view of (a) around the condensate surface.

We repeat the experiments with atom clouds cooled to just above T_{c}. Figure 3(a) shows a cross-section through a cloud containing $N_{\mathrm{T}} = (6.20 \pm 0.05) \times 10^6$ atoms, imaged after 7 ms time-of-flight with +5 MHz detuned probe light. From measurements of the expansion rate of the clouds, we obtain a temperature of $(1.61 \pm 0.03)\,\mu$K. The critical temperature calculated from N_{T} is $1.63\,\mu$K [24]. As can be seen from the figure, there is good agreement between the observed optical density and a model (with no free parameters) of a freely expanding Bose-Einstein cloud with 6.20×10^6 atoms and a chemical potential $\mu = 0$. The χ^2 value is 1.1.

We also cool clouds to near absolute zero, where the fraction of noncondensed atoms is negligible. Pure condensates with $(1.5 \pm 0.1) \times 10^6$ atoms are seen to expand in agreement with predictions based on eq. (1) with $n_{\mathrm{T}}(\boldsymbol{r}, t) = 0$. Figure 3(b) shows a condensate imaged after 8 ms time-of-flight with +10 MHz detuned probe light. The solid curve is the calculated profile with no adjustable parameters and the χ^2 value is 1.1.

Magnetic fields during trap turn-off are found to have visible effects on condensate expansion in the axial (z) direction, but have no effect in the transverse x, y directions. The parameters in our model for eddy currents are fine tuned to account for the observed condensate expansion in the z-direction. It is important to note, however, that the effects of the interaction between condensate and noncondensed atoms are significant only in the transverse directions where the calculated profiles are insensitive to eddy current fields.

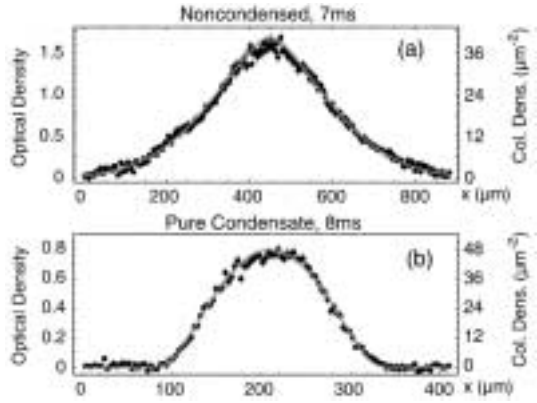

Fig. 3 – (a) Cross-section through a noncondensed cloud of $(6.20 \pm 0.05) \times 10^6$ atoms. The solid curve is obtained for a freely expanding cloud with an initial phase space density given as the Bose-Einstein distribution for 6.20×10^6 atoms and a chemical potential $\mu = 0$. (b) Cross-section through a pure condensate (condensate fraction $> 95\%$) containing $(1.5 \pm 0.1) \times 10^6$ atoms. The solid curve is obtained from a model where the condensate expansion is given by the Gross-Pitaevskii equation (eq. (1)) with no noncondensed component.

The dynamics of the condensate wave function are represented by eq. (1) which includes an additional factor of two in the term $2U_0 n_{\rm T}(\boldsymbol{r}, t)$, describing the interaction of noncondensed atoms with the condensate, as compared to the term $U_0 n_{\rm C}(\boldsymbol{r}, t)$ for interactions within the condensate. This is due to quantum-mechanical exchange effects originating from the requirement of symmetrization of the wave function for identical particles in different quantum states. The front factor for the $U_0 n_{\rm T}(\boldsymbol{r}, t)$ term is related to the factorized part of the second-order correlation function [14] for noncondensed atoms at small distance, $g^{(2)}_{0,\rm NC}(\boldsymbol{r}, \boldsymbol{r} + \boldsymbol{r'}), \boldsymbol{r'} \to 0$. We have performed a rigorous derivation of eq. (1), based on a delta-function approximation for the atomic pair potential. This results in a front factor of $(1 + g^{(1)}_{\rm NC}(\boldsymbol{r}, \boldsymbol{r} + \boldsymbol{r'})), \boldsymbol{r'} \to 0$, where $g^{(1)}_{\rm NC}$ is the first-order correlation function for noncondensed atoms. The factorized part of the second-order correlation function is given by [14]

$$g^{(2)}_{0,\rm NC}(\boldsymbol{r}, \boldsymbol{r} + \boldsymbol{r'}) = 1 + |g^{(1)}_{\rm NC}(\boldsymbol{r}, \boldsymbol{r} + \boldsymbol{r'})|^2 \,. \tag{4}$$

Motivated by this, we have compared the data shown in fig. 1 to a sequence of models where we have varied the value of $g^{(2)}_{0,\rm NC}(0)$ and correspondingly replaced eq. (1) by

$$\begin{aligned} \frac{i\,\hbar\,\partial\Phi(\boldsymbol{r}, t)}{\partial t} \;=\; & \left(\frac{-\hbar^2 \nabla^2}{2m} + V(\boldsymbol{r}, t) + U_0\, n_{\rm C}(\boldsymbol{r}, t) \;+ \right. \\ & \left. + \left(1 + \sqrt{g^{(2)}_{0,\rm NC}(0) - 1} \right) U_0\, n_{\rm T}(\boldsymbol{r}, t) \right) \Phi(\boldsymbol{r}, t) \,. \end{aligned} \tag{5}$$

For the expansion of the noncondensed component, we similarly replaced the interaction potential in eq. (2) by $(1 + \sqrt{g^{(2)}_{0,\rm NC}(0) - 1})\, U_0\, n_{\rm C}(\boldsymbol{r}, t)$. We conclude from our data that $g^{(2)}_{0,\rm NC}(0) = 1.8 \pm 0.3$. This value represents the enhanced probability for finding two noncondensed, identical bosons at small distance as first observed with photons in the Hanbury-Brown and Twiss experiment [26].

In conclusion, we have studied the dynamics of finite-temperature atom clouds which are cooled below the critical temperature for Bose-Einstein condensation and subsequently released from the magnetic trap where they are initially confined. Our observations reveal significant effects on the cloud dynamics from the repulsive interaction between the condensate component and the noncondensed atoms.

* * *

This work was supported by the Rowland Institute for Science. BDB is supported by a Bell Fellowship, and CHB by an NSF fellowship.

REFERENCES

[1] Anderson M. H. *et al.*, *Science*, **269** (1995) 198.
[2] Bradley C. C. *et al.*, *Phys. Rev. Lett.*, **75** (1995) 1687; see also Bradley C. C., Sackett C. A. and Hulet R. G., *Phys. Rev. Lett.*, **78** (1997) 985.
[3] Davis K. B. *et al.*, *Phys. Rev. Lett.*, **75** (1995) 3969.
[4] For a review, see Dalfovo F. *et al.*, *Rev. Mod. Phys.*, **71** (1999) 463.
[5] Griffin A., *Phys. Rev. B*, **53** (1996) 9341.
[6] Giorgini S., Pitaevskii L. P. and Stringari S., *J. Low Temp. Phys.*, **109** (1997) 309.
[7] Jin D. S. *et al.*, *Phys. Rev. Lett.*, **78** (1997) 764.
[8] Stamper-Kurn D. M. *et al.*, *Phys. Rev. Lett.*, **81** (1998) 500.
[9] Hutchinson D. A. W., Dodd R. J. and Burnett K., *Phys. Rev. Lett.*, **81** (1998) 2198.
[10] Fedichev P. O. and Shlyapnikov G. V., *Phys. Rev. A*, **58** (1998) 3146.
[11] Olshanii M., LANL E-Print Cond-Mat/9807412.
[12] Zaremba E., Nikuni T. and Griffin A., *J. Low Temp. Phys.*, **116** (1999) 227.
[13] Ketterle W. and Miesner H. J., *Phys. Rev. A*, **56** (1997) 3291.
[14] Naraschewski M. and Glauber R. J., *Phys. Rev. A*, **59** (1999) 4595.
[15] Hau L. V. *et al.*, *Photonic, Electronic and Atomic Collisions*, in *Proceedings of the XX ICPEAC, Vienna, Austria, 1997*, edited by F. Aumayr and H. P. Winter (World Scientific, Singapore) 1998.
[16] Hau L. V. *et al.*, *Phys. Rev. A*, **58** (1998) R54.
[17] Fetter A. L. and Walecka J. D., *Quantum Theory of Many-Particle Systems* (McGraw-Hill, New York) 1971.
[18] Tiesinga E. *et al.*, *J. Res. Natl. Inst. Stand. Technol.*, **101** (1996) 505.
[19] Wu H. and Arimondo E., *Europhys. Lett.*, **43** (1998) 141.
[20] Hutchinson D. A. W., Zaremba E. and Griffin A., *Phys. Rev. Lett.*, **78** (1997) 1842.
[21] Baym G. and Pethick C. J., *Phys. Rev. Lett.*, **76** (1996) 6.
[22] Fleck J. A., Morris J. R. and Feit M. D., *Appl. Phys.*, **10** (1976) 129; Feagin J. M., *Quantum Methods with Mathematica* (Springer Verlag, New York) 1994.
[23] The interaction with the noncondensed component has very little effect on the expansion of the condensate and we find that the result of the split operator technique can be very precisely represented with an analytical model. We start with the method of Castin and Dum for calculating the condensate expansion with no noncondensed cloud interaction (see Castin Y. and Dum R., *Phys. Rev. Lett.*, **77** (1996) 5315). We introduce a finite healing length at the condensate surface (Dalfovo F., Pitaevskii L. and Stringari S., *Phys. Rev. A*, **54** (1996) 4213) by replacing the first derivative of the Castin-Dum condensate wave function with a product of that derivative and a Fermi function centered at the surface. Since the density profile in the interface region is very sensitive to the exact shape of the condensate surface, it is important to include this smoothing of the condensate density at the surface.
[24] Giorgini S., Pitaevskii L. P. and Stringari S., *Phys. Rev. A*, **54** (1996) R4633.
[25] Huang K., *Statistical Mechanics*, 2nd edition (John Wiley & Sons, New York) 1987.
[26] Hanbury-Brown R. and Twiss R. Q., *Nature*, **177** (1957) 27.